Int. J. Electrochem. Sci., 17 **(2022)** Article Number: 221230, doi: 10.20964/2022.12.40

International Journal of
ELECTROCHEMICAL
SCIENCE
www.electrochemsci.org

Short Communication

Heat treatment improved the corrosion resistance of laser-welded joints of SK5 steel with the notch effect

Chien-Hung Lin[*], *Pei-Jing Teng*

Department of Physics, ROC Military Academy, Feng-Shan, Kaohsiung 830, Taiwan
[*]E-mail: linhungcma@gmail.com

Received: 27 July 2022 / *Accepted:* 14 November 2022 / *Published:* 30 November 2022

A high energy density heat source was a candidate choice for the laser welding of dissimilar steels. A thin heat-affected zone (HAZ) demonstrated the high precision of the laser welding treatment, and the performance was superior to that of traditional arc welding. This investigation examined the tensile deformation behaviour of SK5 steel under constant laser welding parameters, and the electrochemical properties of the joint were also characterized in brine water (3.5% wt NaCl solution). A martensitic structure existed in the fusion zone, and it deteriorated the mechanical performance of the substrate with the welding treatment. Annealing at a temperature of 450 °C for 1 hour was used to promote the performance of the SK5 steel. Meanwhile, the annealing treatment decreased the thermal stresses to inhibit crack initiation from the grain boundary due to diffusion of the carbon atoms in the heat-affected zone. Additionally, the corrosion current densities of the laser-welded specimens with and without the annealing treatment were 2.97×10^{-5} A/cm^2 and 5.97×10^{-6} A/cm^2, respectively. The annealing treatment effectively enhanced the tensile and corrosion resistance of the SK5 steel in brine water. It was demonstrated that dendrite coarsening in the fusion zone effectively enhanced the corrosion resistance of SK5 steel.

Keywords: laser welding, SK5 steel, fusion zone, annealing treatment, corrosion current

1. INTRODUCTION

Geometrical irregularities such as notches result from surface joint welding errors in the welding of dissimilar materials, which deteriorate the tensile and fatigue properties of the materials. The welding quality depends on the shape geometry, structural design, fabrication procedure and heat treatment. Low toughness and strength of a weld joint diminish the equipment life cycle. Serious accidents, such as boiler explosion, tank leakage, bridge collapse and vessel decomposition, have been caused by the failure of weld joints [1-2]. In recent decades, the laser welding technique has been extensively applied in industrial plants, vessel bodies, aerospace fields, vehicle frames, petrochemical industries and pipeline engineering. Hence, the fundamental properties of laser welds have been evaluated in many studies [3-

6]. The welding performance of SK5 tool steel was explored in a brine water environment in this study. According to the results, heat treatment can be used for grain refinement, which improves the chemical and physical properties of weld joints [7-11].

The UTS (ultimate tensile strength) and TF (time to failure) of AISI 316L stainless steel with and without cold work after the welding process were investigated [12]. The TF of the welded specimen decreased with radical transformations in the heat-affected zone, such as recrystallization, sensitization, geometrical coalescence and martensite phase induction at the grain boundary. Furthermore, work hardening enhanced the UTS of 316L stainless steel in ambient air. The specimen exhibited stress corrosion initiation at the initial stage and accelerated rupture under corrosive conditions. The mechanical properties of laser-welded AISI 304L stainless steel with heat treatment at 200 and 400 ℃ were investigated [13]. The relief of residual stress sufficiently promoted the corrosion resistance and tensile strength of the weld joint after heat treatment at 200 °C. However, the segregation of compounds, such as FeNi, Ni_3Ti, Fe_2Ti, and Cr_2Ti, deteriorated the performance of the weld joint when an annealing treatment was conducted at 400 ℃ for 1 hour. Obviously, superior performance of the weld joint was obtained after the annealing treatment under suitable conditions. The interaction of the welding parameters, such as the welding speed and laser power, enhanced the tensile performance of the weld joint [14]. The microstructure of the cross-section illustrated that the geometry was strongly related to the welding speed. The microhardness value progressively descended from the substrate to the centerline of the fusion region. Coarse grains were obtained in the fusion region at a low cooling rate, while the scan speed was dominant at a slow rate. A heterogeneous interface appeared between the base metal and fusion zone after the welding process, and it demonstrated brittle behaviour on the fractography evaluation after the tensile test. The stable passive layer on the fusion zone promoted the corrosion resistance of the weld joint during the precipitation of Ti/Ni in the present study.

Ferritic stainless steel (FSS) and low-carbon steel (CS) were employed for dissimilar joint welding, and scan speeds of 12 mm/s and 24 mm/s, respectively, were utilized [15]. The width of the heat-affected zone was strongly correlated with the welding speed on substrates, and the microhardness of ferritic stainless steel increased with the scan speed. The ductility of the joint was predominantly related to the scan speed. The longer residence of heat promoted Cr and Fe diffusion to the heat-affected zone, and superior elongation was obtained at 24 mm/s because less heat was preserved in the fusion zone. Furthermore, the corrosion resistance of the weld joint of ferritic stainless steel and low carbon steel decreased due to galvanic corrosion in the brine water. The relationship between the properties of the weld joint and the manipulation parameters was discussed by [16]. The results demonstrated that the laser power, scanning rate and laser focus were strongly correlated with the tensile resistance of the weld joint. Pinholes, cracks and other defects formed in the heat-effected zone due to the use of unsuitable parameters. The tensile strength and harness were dependent on the recrystallization and annealing temperatures.

The notch effect resulted from surface welding errors, which created stress concentrations on the tensile specimen [17-20]. The laser welding technique has been widely discussed in many studies [21], but identifying the relationship between the notch effect and performance has become a practical problem in engineering. Hence, the objective of this study was to investigate the failure behaviour of

SK5 steel in brine water under the notch effect. Improving the mechanical performance of SK5 steel in brine water is a crucial issue for broadening the practical application.

2. EXPERIMENTAL METHOD

2.1 Specimen preparation

SSRT (slow strain rate testing) was employed to determine the mechanical properties of the experimental specimen (according to ASTM D638). The gauge area was 2.5 mm thick, and the geometry of the specimens is shown in Fig. 1. The chemical composition of SK5 steel is presented in Table 1. The substrate was pretreated with ethanol and dehydrated at 65 °C for 1 hour before the welding process.

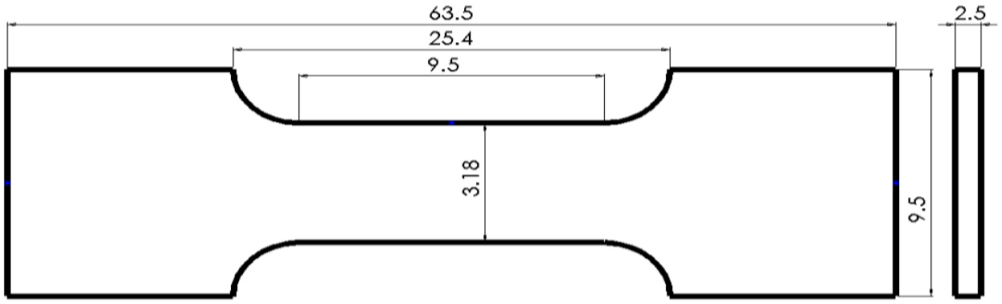

(a) Dimensions of the tensile specimen, unit: mm

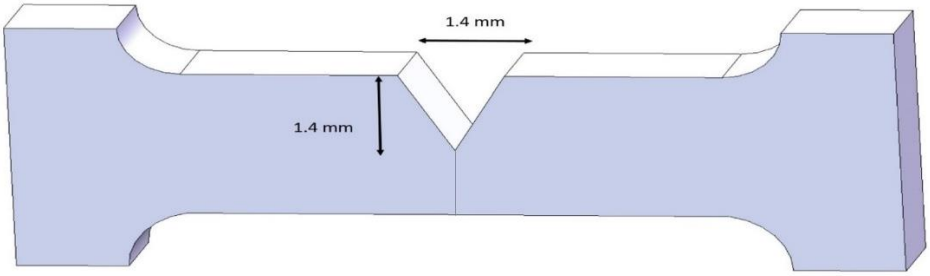

(b) Geometry of a single edge notched specimen with a V notch.

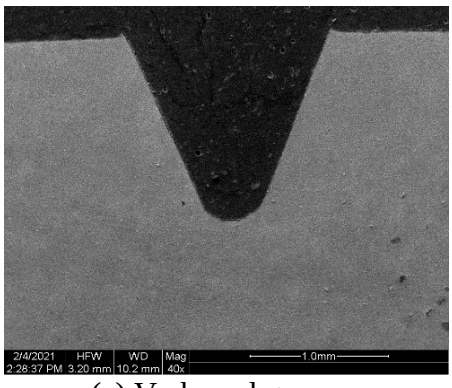

(c) V-shaped groove.

Figure 1. Schematic diagram of tensile specimens that obeyed the ASTM D638 standard: (a) Dimensions of the original specimen, (b) dimensions of the V-notch specimen, and (c) SEM morphology of the V-shaped groove.

A V-notch groove was machined on the plate to evaluate the notch effect of the specimen, as shown in Fig. 1(b-c). Furthermore, the specimen was treated at an annealing temperature of 450 °C for 1 hour to investigate the performance of the specimen after the heat treatment.

Table 1. Chemical composition of SK5 steel. (wt%)

Element	C	Si	Mn	S	P
weight%	0.8	0.2	0.15	0.025	0.025

A laser light beam with a high power density was employed for joint welding, which was conducted using a Nd:YAG (yttrium aluminium garnet) pulsed laser welding machine (Yao Hung Technology Co., Ltd.). The manual parameters for laser welding were chosen based on the material, depth and geometry of the joint. The welding speed, focal point position, laser power and shielding gas were fixed to ensure the consistency of the welding quality [14-15]. A laser power of 2 kW, a laser beam diameter of 1.0 mm and a scanning speed of 2 mm/sec were utilized, as presented in Table 2. Meanwhile, the focal point position relative to the upper side of the specimen was -1 mm. Argon gas was employed as the shielding gas with a pressure of 2 MPa to avoid oxidation of the molten metal on the SK5 steel, and the optimal flow rate of the shielding gas was used to reduce the dissipation behaviour of the ionic plasma.

Table 2. Laser welding process parameters of SK5 steel.

Parameters	Power	Beam diameter	Position	Welding speed	Argon Pressure
Value	2(kW)	1(mm)	-1(mm)	2(mm / sec)	2(MPa)

2.2 Slow strain rate test

The laser-welded specimens were loaded into a tension clamp at room temperature under a low strain rate (5.5×10^{-7} sec^{-1}). Meanwhile, the stress corrosion cracking susceptibility of each welded joint was evaluated in brine water [12, 16]. The slow strain rate test was employed to characterize the stress–strain response characteristics of each laser-welded specimen, such as the ultimate strength, elongation rate and yield behaviour. The experimental apparatus used in the present study is illustrated schematically in Fig. 2.

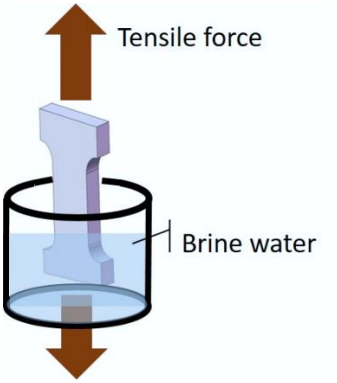

Figure 2. Diagram of the experimental apparatus for tensile testing performed at ambient temperature (strain rate 5.5 x $10^{-7}sec^{-1}$).

2.3 Corrosion test

A potentiodynamic polarization test was executed to evaluate the corrosion resistance of the SK5 steel in a 3.5% wt NaCl solution [6, 20]. The specimen was electrochemically monitored using a Versastat 4 device (AMETEK Inc), and the electrochemical performance was characterized by the Tafel slope, corrosion current and potential. The SK5 steel was employed as the working electrode in a three-electrode system. Furthermore, Ag/AgCl and platinum were used as reference and auxiliary electrodes, respectively. The standard dimension of the gauge area was 1 cm^2 for the polarization test. The potentiodynamic polarization test was performed from −0.8 V to -0.2 V with respect to the open circuit potential, and the scan rate was fixed at 0.5 mV/s. The polarization test was ended when the current density exceeded 2 mA/cm^2.

3. RESULTS AND DISCUSSION

3.1 Microstructure and hardness

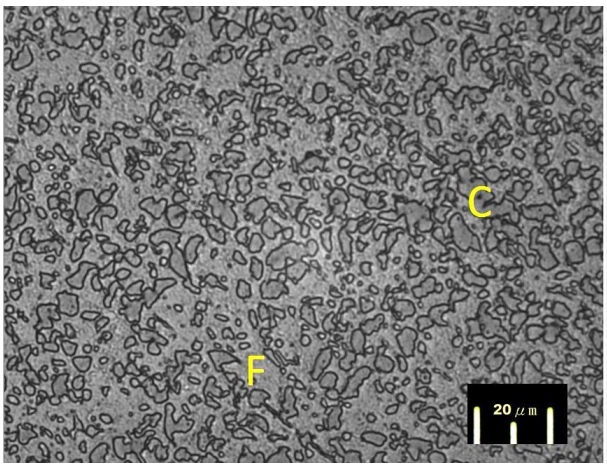

(a) Metallographic image of SK5 steel. C: cementite phase and F: ferrite.

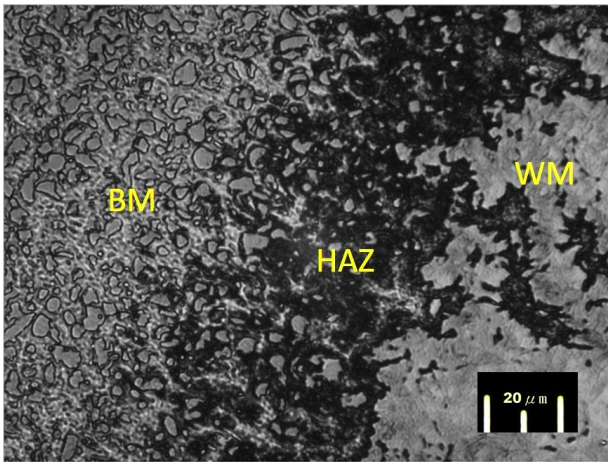

(b) Image of the as-welding SK5 steel specimen. WM: weld metal zone, BM: base metal zone, and HAZ: heat-affected zone.

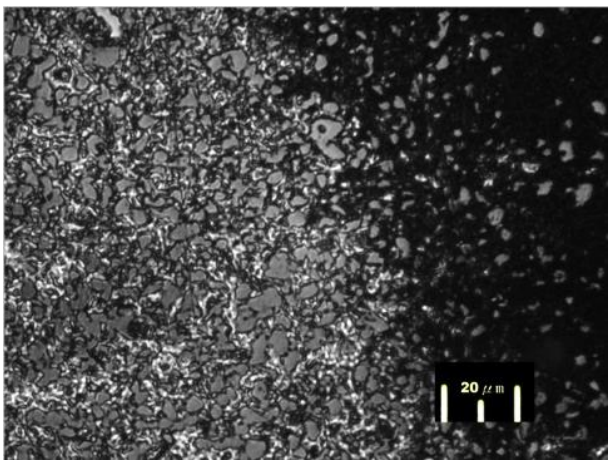

(c) Microstructure between the fusion and base metal boundaries of the SK5 steel specimen with heat treatment

Figure 3. Metallographic images of the SK5 steel specimen: (a) substrate, (b) as-welding specimen, (c) with annealing treatment (temperature of 450 °C for 1 hour).

The specimen was polished with silicon carbide papers (from 400 to 2000 grade), cleaned with distilled water and dehydrated at 65 °C in an oven. The metallography was observed after an etching treatment in 8 wt% nitric acid mixed with the ethanol. The globular cementite phase embedded in the ferrite base is presented in the metallographic images in Fig. 3(a). The microstructure of the welding joint demonstrated a significant discrepancy after the laser welding treatment. The laser beams heated the base metal beyond its melting point within a few milliseconds, and the weld metal returned to the ambient temperature rapidly. The hardness obviously decreased from the weld zone towards the base metal, as shown in Table 3. The microstructure consisted of the weld metal (WM), the base metal (BM) and the heat-affected zone (HAZ), as shown in Fig. 3(b). The width of the heat-affected zone decreased after the annealing treatment, as shown in Fig. 3(c), and the carbon atom completely diffused from the WM to the HAZ [7-8].

The cells transformed into dendrites due to the rapid cooling rate, and an unstable interface existed in the transverse direction. Hence, the carbon atoms showed decreased diffusion ability in the grain boundary due to insufficient time. The morphology transformed from cellular to dendritic, as shown in Fig. 4(b-c), and the amount of dendrites strongly increased with the solidification of the weld metal zone [20]. The average microhardnesses of the weld metal and the base metal were 803 Hv and 166 Hv, respectively. Furthermore, the Vickers hardness of the transitional phase for the heat affected zone was 326 Hv averaged over every 5 points, as presented in Table 3. The heat treatment at an annealing temperature of 450 °C for 1 hour enhanced the stress-relief effect of the SK5 steel, and the carbon atoms diffused with sufficient time [15, 18]. The Vickers hardnesses of the WM and BM decreased to 237 Hv and 142 Hv, respectively.

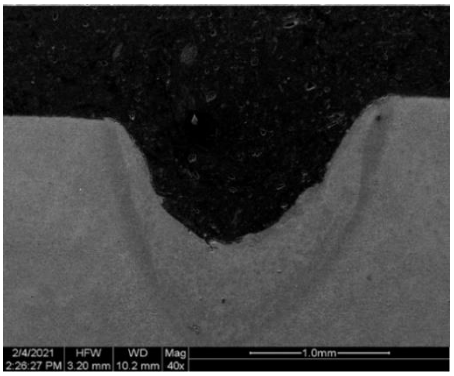

(a) Transverse section of the SK5 steel with laser welding

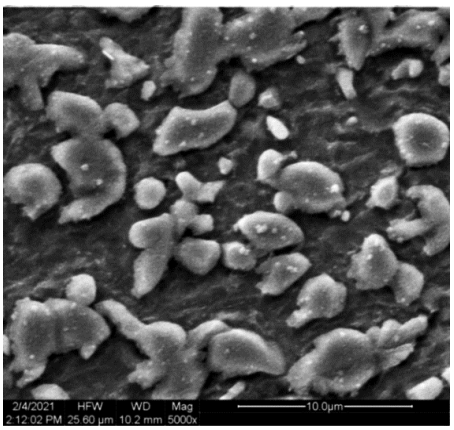

(b) Base metal zone

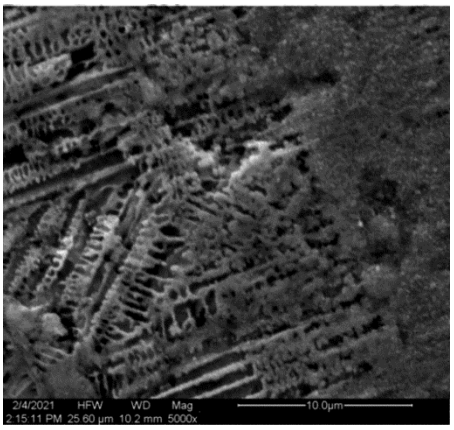

(c) Weld metal zone

Figure 4. SEM morphology of the SK5 steel with and without the laser welding treatment: (a) Cross-section, (b) base metal zone, and (c) weld metal zone

Table 3. The Vickers hardness of the SK5 steel with and without the annealing treatment.

Vickers Hardness(HV)							
Mode	Zone	1	2	3	4	5	Mean
As-welding	BM	173	182	196	164	195	182
	HAZ	350	318	310	325	327	326
	Fusion zone	815	839	789	753	819	803
Annealing	BM	180	122	143	126	139	142
	HAZ	269	218	208	252	238	237

3.2 SSRT

A stress–strain diagram was employed to characterize the performance of the SK5 steel in brine water. The yield phenomenon was accompanied by significant plastic strain as the continual stress reached a critical level [5]. The ultimate strengths of the specimens with and without laser welding treatment were 645 MPa and 575 MPa, respectively. The high-density martensitic structure was widely distributed in the microstructure at the weld metal zone, which enhanced the hardening mechanics (Fig. 4(c)). There was insufficient time for the carbon atoms to diffuse into the crystal structure, and the phase transformed to martensite after the laser welding treatment [12]. The heat moved rapidly from the weld metal region into the base metal, and the formation of fine grains was caused by the rapid cooling rate, as described in Section 3.1. The internal stress concentrated in the grain boundary acted as martensite to strengthen the hardening mechanics [4]. Meanwhile, dislocations abundantly accumulated in the martensite, and the dislocation strain energy enhanced the deformation resistance of the SK5 steel.

However, the hardened mechanics decreased the elongation rate of the SK5 steel. The welded joint exhibited a lower elongation rate (3.5%) than the substrate with the V-notch (5.1%), as shown in Fig. 5(a). Hence, an annealing treatment was employed to reduce the residual stress after laser welding. The grain size increased in the weld metal zone after annealing at 450 °C for 1 hour, and then the thermal and residual stresses were released in the SK5 steel.

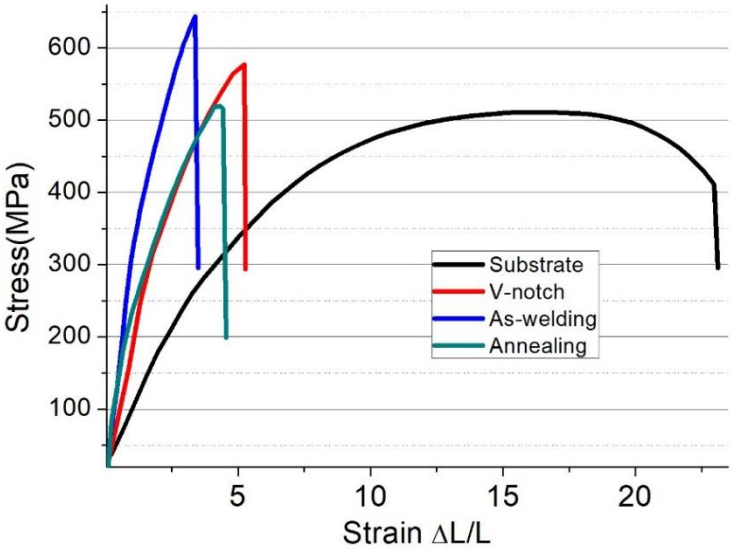

(a) Measured in ambient air

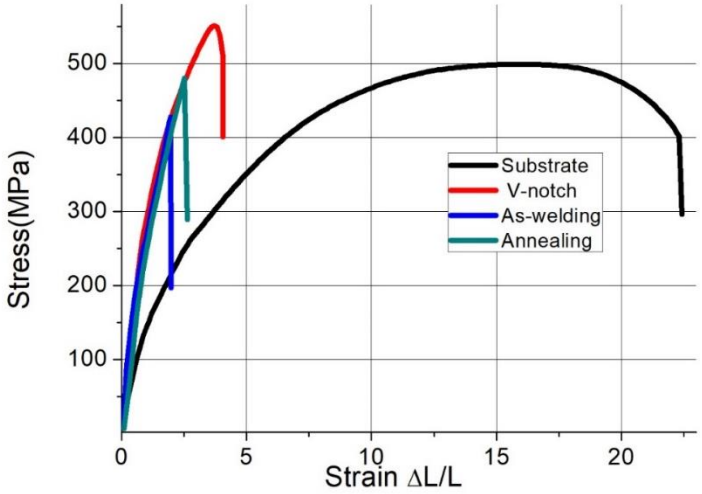

(b) Measured in a 3.5% wt NaCl solution

Figure 5. Stress–strain curves (Strain rate: $5.5x10^{-7}$ sec^{-1}) of the SK5 steel (a) in ambient air and (b) in a 3.5% wt NaCl solution. The annealing treatment performed at 450 °C for 1 hour to enhance the stress-relief effect of the SK5 steel after the welding process.

Quenching cracking from the grain boundary was inhibited, and the elongation rate was promoted because there was sufficient time for the carbon atoms to diffuse in the structure [2]. The annealing treatment effectively enhanced the toughness of the SK5 steel in brine water by approximately 30% after the heat treatment, as shown in Fig. 5(b). Further, the formation of a reinforced phase was induced by the coarse grains on the SK5 steel with the annealing treatment, which increased the

toughness, and the slender HAZ enhanced the corrosion resistance of the tensile specimen in brine water [6, 20]. Meanwhile, the elongation rates of the specimens with and without the annealing treatment were 2.6% and 2.0%, respectively.

3.3 Corrosion test

The current profile was employed to provide the relative ranking of the corrosion resistance for each joint, as shown in Fig. 6, and the scan rate of the potentiodynamic curve was fixed at 0.3 mV/s. The corrosion current density (i_{corr}) of the specimens at the substrate was 1.84×10^{-7} A/cm^2 in brine water (3.5 wt% NaCl) as Table 4. The i_{corr} value of the SK5 steel specimen after welding was 2.97×10^{-5} A/cm^2, which was obviously higher than that of the SK5 steel specimen after welding with the annealing treatment, namely, 5.97×10^{-6} A/cm^2. The SK5 steel with welding treatment shifts E_{corr} towards negative values and reduces the I_{corr} (corrosion current density) of the SK5 steel substrate by 1 order of magnitude. The corrosion rate increased with the laser welding treatment due to the fine grain size and the presence of martensite in the structure after the laser welding treatment [8, 21], as described in Section 3.1. However, the corrosion resistance of the laser-welded specimen increased with the annealing treatment, which was due to the coarse grains and the extinguishment of the heat-affected zone in the structure [3]. The inferior corrosion resistance of the as-welding joint compared to the specimen with the annealing treatment can be attributed to the precipitation characteristics of carbon atoms in the heat-affected zone.

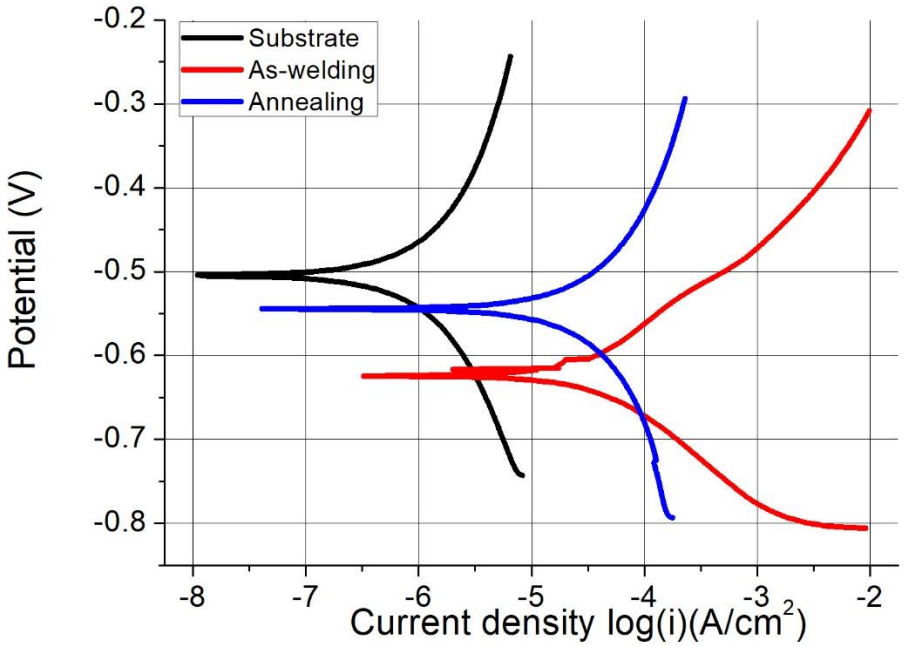

Figure 6. Polarization curves (sweeping potential from −0.85 V to -0.25 V) of the SK5 steel specimen in brine water (3.5 wt% NaCl solution) at ambient temperature. The corrosion resistance of as-welding and annealing specimen obtained by the welding joint with and without heat treatment (temperature of 450 °C for 1 hour).

Table 4. Corrosion characteristics of SK5 steel with and without annealing treatment in a 3.5 wt% NaCl solution by polarization measurements. E_{corr} and I_{corr} denote corrosion potential and corrosion current density of the SK5 steel, respectively.

Specimen	E_{corr}(V) $_{vs}$ SCE	I_{corr}(A/cm^2)
Substrate	-0.504	1.84E-7
As-welding	-0.624	2.97E-5
Annealing	-0.544	5.97E-6

3.4 Fracture surface of the SSRT specimen

The fracture behaviour of the specimen was observed by optical microscopy. The crack propagation was predominantly determined by the structural parameter. The tough specimen absorbed excess energy and exhibited plastic behaviour before the failure stage. Hence, the substrate demonstrated necking behaviour, and the transverse length was obviously reduced, as shown in Fig. 7(a). Meanwhile, the crack path was perpendicular to the direction of the loading force, and a smooth profile was demonstrated on the transverse section of the substrate due to its V-notch shape, as shown in Fig. 7(b). A stress concentration region existed in the V-notch, and it shrunk when the tensile force was above a critical value. It was proven that a quasi-brittle deformation was induced by the machining of the V-notch on the specimen.

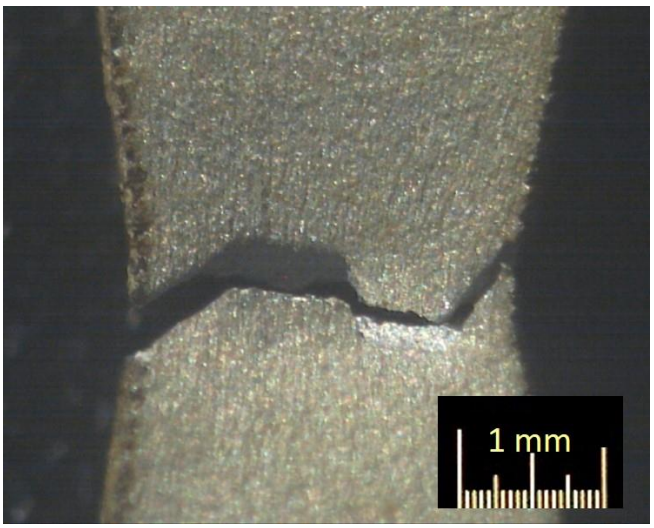

(a) Necking behaviour of the substrate

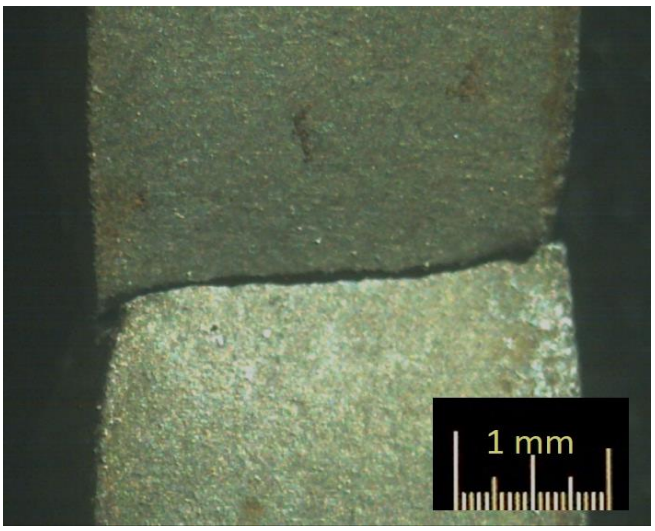

(b)V-notched specimen

Figure 7. Transverse section of the fracture surface from SK5 steel in an ambient atmosphere (strain rate 5.5 x $10^{-7}$$sec^{-1}$).

The fracture surfaces of the welded specimens with and without the annealing treatment are shown in Fig. 8. After the SSRT, the elongations were approximately 3.5% and 5.1% for the welded specimens with and without the annealing treatment, respectively. Meanwhile, the elongation of the specimen with the annealing treatment was superior to that of the as-welding specimen. The diffusion of carbon to dislocations after the welding treatment was responsible for strain ageing and brittleness [12]. The residual stress was caused by the thermal gradient at the welding stage and the rapid cooling below the equilibrium melting temperature, which enhanced the driving force for solidification. The tensile fracture surface of the as-welding specimen, which shows cleavage and brittle fracture features, is presented in Fig. 8(a). Moreover, crack initiation was inhibited by the relief of the residual thermal stresses after the annealing treatment. The tensile fracture surface exhibited a serration pattern [13], and mixed ductile–brittle fracture features were observed in the welding specimen with the annealing treatment, as shown in Fig. 8(b).

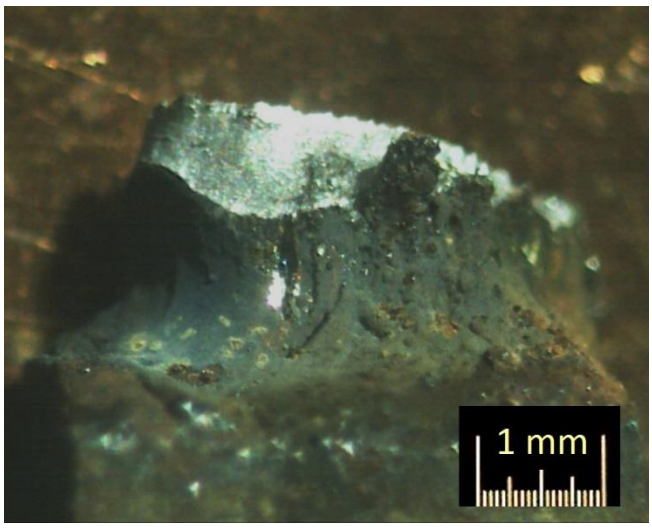

(a) As-welding sample

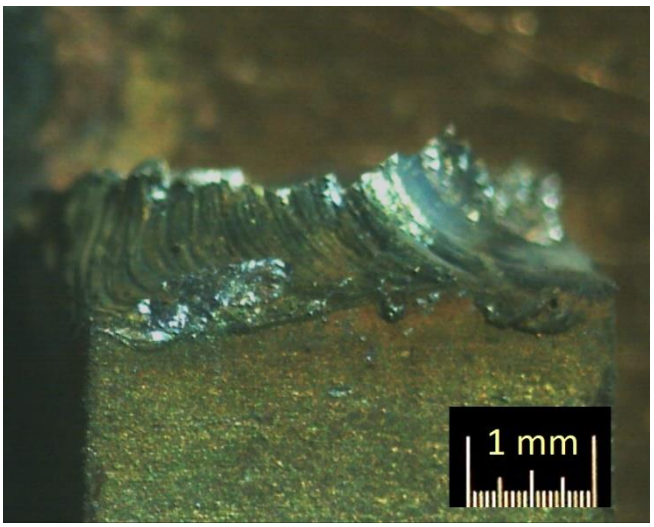

(b) Annealing treatment

Figure 8. Fracture surfaces of the as-welding and annealed SK5 steels with SSRT (strain rate 5.5 x $10^{-7}$$sec^{-1}$) in an ambient environment.

4. CONCLUSIONS

The laser welding technique was applied to SK5 steels, and a slender joining area was demonstrated on the specimen in this paper. To examine the notch effect, a geometrical V notch was preshaved on an SK5 steel specimen before laser welding. A high-density martensitic structure was distributed in the weld metal zone, which enhanced the hardening mechanics; however, it deteriorated the ductility of the SK5 steel due to the nonuniform distribution of carbon atoms in this zone. Residual stress was relieved after an annealing treatment (at 450 °C for 1 hour), and the elongation rate was enhanced with less martensite. Furthermore, the i_{corr} value of SK5 steel with the annealing treatment was 5.97×10^{-6} A/cm^2, which was obviously lower than that of the as-welding specimen (2.97×10^{-5} A/cm^2) due to the presence of coarse grains. Hence, the annealing treatment effectively enhanced the toughness and corrosion resistance of the SK5 steel in brine water by approximately 30% and one order of magnitude, respectively. According to the obtained fracture diagram, the SK5 steel exhibited mixed ductile–brittle fracture features because the width of the heat-affected zone decreased after the annealing treatment. Future research is required to investigate the relationship between the heat treatment conditions (temperature and time) and the mechanical properties of SK5 steel in liquid environments.

ACKNOWLEDGEMENTS
The authors acknowledge material support provided by the Yao Hung Technology Co., Ltd. of the Republic of China.

References

1. K. D. Ramkumar, W. S. Abraham, V. Vedha Viyash, N. Arivazhagan, A. M. Rabel, *J. Manfu. Process.*, 25 (2017) 306.
2. Z. H. Fu, G. Q. Gou, Z. Y. Zhu, C. P. Ma, W. Q. Yang, L. L. Zhang, Y. C. Hu, W. Gao, *Corros. Sci.*, 143 (2018) 23.
3. E. F. Pieretti, E. J. Pessine, O. V. Correa, W. Rossi, M. D. M. Neves, *Int. J. Electrochem. Sci.*, 10 (2015) 1221.
4. C. Köse, *Int. J. Electrochem. Sci.*, 11 (2016) 3542.
5. Y. Liu, S. Tang, G. Liu, Y. Sun, J. Hu, *Int. J. Electrochem. Sci.*, 11 (2016) 10561.
6. M. C. Ramírez-López, L. A. Falcón-Franco, F. F. Curiel-López, P. Zambrano, J. A. Cabral-Miramontes, C. Gaona-Tiburcio, F. Almeraya-Calderón, *Int. J. Electrochem. Sci.*, 12 (2017) 4928.
7. J. Sun, X. Li, Y. Sun, Y. Jiang, J. Li, *Int. J. Electrochem. Sci.*, 13 (2018) 11607.
8. Ce. KÖSE, *Int. J. Electrochem. Sci.*, 13 (2018) 12208.
9. M. Yang, H. Yang, L. Yang, Y. Liu, J. Tan, J. Chen, *Int. J. Electrochem. Sci.*, 15 (2020) 280.
10. Y. Liu, J. Feng, S. Tan, Y. Cheng, J. Hu, *Int. J. Electrochem. Sci.*, 15 (2020) 9204.
11. X. Cao, B. Rivaux, M. Jahazi, J. Cuddy, A. Birur, *J. Mater. Sci.*, 44 (2009) 4557.
12. P. D. Tiedra, Ó. Martín, *Mate. Des.*, 49 (2013) 103.
13. G. R. Mirshekari, A. Saatchi, A. Kermanpur, S. K. Sadrnezhaad, *J. Mater. Eng. Perform.*, 25 (2016) 2395.
14. S. Datta, M. S. Raza, P. Saha, D. K. Pratihar, *Mater. Manfu.*, 34 (2019) 648.
15. W. Wu, S. Hu, J. Shen, *Mater. Des.*, 65 (2015) 855.
16. L. F. Mei, J. M. Yi, D. B. Yan, J. W. Liu, G. Y. Chen, *Mater. Des.*, 40 (2012) 433.
17. Z. L. Zhang, M. Hauge, C. Thaulow, J. Ødegard, *Eng. Fract. Mech*., 69 (2002) 353.
18. A. K. Lakshminarayanan, V. Balasubramanian, *Mater. Des.*, 31 (2010) 4592.
19. R. T. Qu, P. Zhang, Z. F. Zhang, *J. Mater. Sci. Technol.*, 30(2014), 599.
20. M. Yang, J. Lu , Y. Li, J. Tan, W. Zhang, H. Yang, *Int. J. Electrochem. Sci.*, 15 (2020) 9811.
21. C. Sung, B. H. Shin, W. Chung, *Int. J. Electrochem. Sci.*, 17 (2022) 220339.